International Journal of Control, Automation, and Systems 21(4) (2023) 1243-1257
http://dx.doi.org/10.1007/s12555-021-0972-5
ISSN:1598-6446 eISSN:2005-4092
http://www.springer.com/12555

Disturbance Observer-based Neural Network Integral Sliding Mode Control for a Constrained Flexible Joint Robotic Manipulator

Quanwei Wen, Xiaohui Yang*, Chao Huang, Junping Zeng, Zhixin Yuan, and Peter Xiaoping Liu

Abstract: In this paper, the tracking control problem of flexible joint robotic manipulator (FJRM) system subjected to system uncertainties and time-varying external disturbances (TVED) is addressed. A new disturbance observer-based neural network integral sliding mode controller with output constraints (DNISMCOC) that comprises the merits of neural networks, disturbance observer and integral sliding mode is proposed. Considering that the radial basis function neural network (RBFNN) has a fast learning convergence speed and great approximation ability, two matrices of RBFNN are utilized to estimate the parameter matrices of the dynamic model of FJRM. In view of the estimation errors of RBFNNs and TVED in the system, a disturbance observer is introduced to estimate the lump uncertainties which consist of them. Integral sliding mode is introduced for eliminating steady errors further. For ensuring security in some high-accuracy using occasions, a barrier lyapunov functions (BLF) is adopted to achieve output constraints of FJRM. To validate the effectiveness of the proposed control scheme, numerical simulations on 2-link FJRM are conducted. According to the comparisons among DNISMCOC and other state-of-the-art controllers, the superiorities of DNISMCOC in several aspects are proved.

Keywords: Backstepping control, disturbance observer, flexible joint robotic manipulator, neural network, output constraints.

1. INTRODUCTION

In recent decades, increasingly attentions have been paid on FJRM since they have been widely used in space and deep-sea exploration, Industrial manufacturing, medical treatment, etc [1-5]. Compared with the traditional rigid joint manipulator, FJRM has advantages of lightweight, small volume, low energy consumption, and high load-to-weight ratio. Moreover, owing to the joint of robotic manipulator is flexible, security is dramatically improved. When FJRMs are happened to be stricken, the flexible joints can alleviate the collision all the time [6]. Even if the FJRM possesses a great deal of superiorities, there is still several challenges the researchers in this field have to face. One of them is how to compensate the mismatched uncertainties that can't directly compensated by actual control input. Another one is the problem of "explosion of complexity" which is inherently arose by the character of high-order of the controlled system of FJRM. Certainly, tracking accuracy and robustness are still the goals researchers pursue to improve.

It is noteworthy that, comparing with the rigid joint robotic manipulator, the control scheme design for the FJRM is not yet mature. As we all know, FJRM is a complicated dynamic system, there are many parameters in its model-based controller [7-9]. What is more, some parameters are not easy to acquire under certain conditions. Thus, researchers have been considering a method that can reduce the requirement of robot parameters in feedback control. In recent years, the application of neural network (NN) has attracted the attentions of the researchers for their merits of learning capability mapping and parallel processing [10-13]. In past decades, unremitting endeavor has been made for exploring NN controllers for FJRM. Authors of [7,14] introduce RBFNN to control FJRM, but both of them simply use it to approximate a large complicated term, which will to some extent increase the difficulties of approximating and lower the tracking accuracy. Authors of [15] use numerous RBFNNs to approximate the uncertain parameter matrices in the dynamic model of FJRM which can in a way overcome the above difficulties and makes RBFNN easier to combine with other control technique.

In most preceding researches of RBFNN control, the

Manuscript received November 17, 2021; revised March 22, 2022; accepted June 5, 2022. Recommended by Associate Editor Xiangpeng Xie under the direction of Senior Editor Bin Jiang. This work is supported by the National Natural Science Foundation of China (51765042, 61963062).

Quanwei Wen, Xiaohui Yang, Chao Huang, Junping Zeng, and Zhixin Yuan are with the College of Information Engineering, Nanchang University, Nanchang 330031, Jiangxi, China (e-mails: 673226821@qq.com, yangxiaohui@ncu.edu.cn, {360553696, 577913498, 2659020678}@qq.com). Peter Xiaoping Liu is with the Department of Systems and Computer Engineering, Carleton University, Ottawa, ON K1S 5B6, Canada (e-mail: xpliu@sce.carleton.ca).
* Corresponding author.

weight estimation update law of RBFNN depends significantly on tracking errors and momentary estimated data, so the convergence of system estimation errors in RBFNN control can't be achieved. Besides, for the TVED, RBFNN is not good enough to compensate it.

In most of the trajectory tracking control literatures, disturbance observer (DO) is a effectively used technique for handling TVED problem [16-20], which can achieve finite time convergence of estimation errors. Moreover, it can also compensate the approximating errors of RBFNN and make up its disadvantage of unable to converge. As a consequence, designing an RBFNN-DO united control law is desirable [21]. In [16], a sliding mode disturbance observer is designed for nonlinear system. In [22], a terminal sliding mode disturbance observer (TSMD) is designed for FJRM. Authors of [23] design an adaptive disturbance observer for nonlinear system. Yet, all of these DOs contain too many parameters to combine well with RBFNN. Besides, the sign function terms and fractional power in these DOs are more likely to generate singularity. In [24], in the condition of guaranteeing the same level of precision, a DO with less parameters and more simplified form is proposed.

Usually, the most prevalent techniques of controller design in FJRM control are fourth-order backstepping control design method [25-27] and fourth-order dynamic surface control design method [26]. Both of them require designers to differentiate a state variable four times for obtaining three virtual control laws and an actual control input. Multiple times of differentiation will increase the risk of instability of this system. Authors of [28] introduce a new backstepping control design method for FJRM where the whole control scheme only includes one virtual control law and an actual control input. This method effectively decreases the times of differentiation during the process of controller design, yet simply using linear sliding surface (LSS) for controlling, which clearly has room for improvement. As is well-known, although sliding mode control (SMC) is a popular control technique for its strong robustness [29,30], there are still several drawbacks such as chattering issue and problem of finite-time convergence that limit its performance in real applications. To solve these difficulties, previous works [31,32] chose fast terminal sliding mode for achieving fast convergence and chattering elimination; Authors of [33] use high order sliding mode (HOSM) for realizing finite-time convergence; Authors of [34] use a integral sliding mode for implementing fast convergence as well as reduction of steady-state errors.

In addition, it's worth noting that plenty of contributions have been made to cope with input saturation problem [35,36], yet the attentions paid on output constraints are not adequate. In practical applications such as health care tasks [37], for protecting patients from accidental injuries of FJRM, output constraints are extremely essential. In [38], a BLF is introduced to implement output constraints with remarkable results, which inspired us to try it in FJRM.

In this paper, motivated by the above discussions, DNISMCOC is proposed to resolve the tracking control problem of n-link FJRM under the circumstance of model uncertainties and TVED. Specifically, DNISMCOC uses RBFNN to estimate the model uncertainties of the system, uses DO to estimate TVED and compensate for the estimation errors of RBFNN, uses BLF to limit the error range of the control outputs to ensure safety in practical use. Compared with [10,12,13,15] that only use RBFNN for approximation and can't precisely estimate TVED, DNISMCOC combines the merits of DO and RBFNN and enables accurate estimation of TVED and convergence of the system estimation errors. Unlike [7,10,12-14] that just use one RBFNN to approximate a complicated term in control law, DNISMCOC uses two matrices of RBFNN to approximate uncertain matrices in dynamic model of FJRM, which will improve the tracking accuracy and makes it more flexible to combine with other techniques. Compared with [14,28] that employ traditional LSS to design control law, DNISMCOC makes use of integral sliding surface (ISS) to improve the speed of convergence and lower the steady state errors one step further. Unlike [25-27,39] that employ commonly used fourth-orders backstepping control method to design control law, DNISMCOC introduces a new backstepping design method which successfully reduces the times of differentiation during the process of controller design and significantly alliviates the problem of "explosion of complexity".

In general, the main contributions of this paper compared to existing work are as follows:

i) The proposed control technology put forward a RBFNN-DO united control method which not only can reduce the parameter information we have to know during the controller design by use of RBFNN but also can make up the shortcoming that estimation errors of RBFNN can't asymptotically converge by use of DO and decrease the estimation errors further.

ii) The proposed new scheme uses two matrices of RBFNN to approximate the uncertain matrices in the dynamic model of FJRM which makes the tracking results more accurate than commonly used one-RBFNN estimation method and facilitates RBFNN combining with other techniques in the process of controller design.

iii) An ISS is involved in control law design, which does a great favor to improve the speed of convergence and decrease the steady state errors.

iv) A new backstepping design method for FJRM is introduced, which successfully reduces the times of differentiation for virtual control law and significantly

alleviates the problem of "explosion of complexity" by means of dividing the controlled system into two subsystems.

The rest of the paper is organized with the following structure. In Section 2, the dynamic model of FJRM and the techniques in the main contributions are present. Section 3 states the process of designing DNISMCOC. Simulation results are shown in Section 4 to verify the effectiveness and superiority of DNISMCOC and some comparisons with other advanced controllers are also made in this part. In Section 5, some conclusions are given.

2. PROBLEM STATEMENT AND PRELIMINARIES

2.1. Preliminary control design

In terms of rigid joint robotic manipulators (RJRM), the conduction from τ to terminal actuator q is straightforward. Therefore, it is easy for researchers to cope with their relationship through either the adaptive control technique or the NN control scheme.

However, different from the widely used dynamic model of RJRM, in the model of FJRM, for taking joint distortion in practical application into account, the angle position of a joint is separated in two part, which are position in link side (angle of link) and position in motor side (angle of motor shaft). These two joint sides are connected through a spiral spring and torque is conducted by torsional deformation of the spiral spring. Therefore, the simplified physical model of FJRM can be described as two-angle-one-spring model which is precisely illustrated in Fig. 1. In this paper, the manipulator is assumed to be a n-DOF (degree of freedom) manipulator with joint flexibility, its nonlinear dynamic model is defined by the following:

$$M(q)\ddot{q}+C(q,\dot{q})\dot{q}+G(q)+F(q,\dot{q}) = K(q_m-q)+\tau_d(t), \tag{1}$$

$$J_m\ddot{q}_m+K(q_m-q)=\tau, \tag{2}$$

where $q \in R^n$ and $q_m \in R^n$ denote the angular positions of the link side and the motor shafts side, respectively.

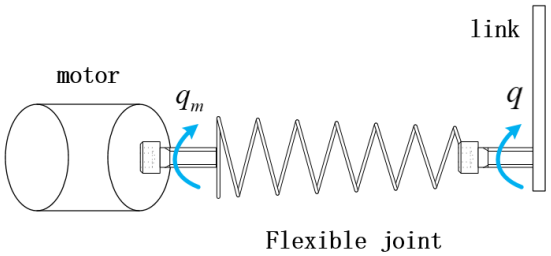

Fig. 1. Model of FJRM.

$M(q): R^n \to R^{n\times n}$ is the symmetric positive definite inertia matrix of the rigid links. $C(q,\dot{q})\dot{q}: R^n \times R^n \to R^n$ represents the coriolis and centrifugal force matrix. $G(q): R^n \to R^n$ denotes the gravitational force. $F(q,\dot{q}) \in R^n$ denotes the friction torques. $\tau \in R^n$ represents the external input torque vector. $\tau_d(t) \in R^n$ denotes the unknown time-varying external disturbances in motor shafts side and link side. $J_m \in R^{n\times n}$ is the positive definite diagonal matrix of the moments of inertia of the motors, and $K \in R^{n\times n}$ is the positive definite diagonal matrix representing the spring stiffness of n joints.

Remark 1: From (1) and (2), it is obvious to find that the dynamic model of FJRM is a fourth-order system where q, $\dot{q}$, q_m, $\dot{q}_m$ are set as its state variables in each layer. Usually, backstepping control method is introduced to control such a higher order nonlinear system and is able to resolve the indirect mapping issue between τ and q, which means q must be differentiated for four times to complete the whole control law design. The multiple differentiation makes the control method more unstable and prone to singularities.

To solve this problem, the dynamic model of FJRM is divided into two subsystems in this paper. The first subsystem is called the link-side subsystem and is represented by (1), where a new variable q_{md} is set as the virtual control law and also denotes the desired trajectory of q_m. q_{md} forces q to track the final ideal trajectory q_d. The second subsystem, called the motor-side subsystem, is dominated by the actual control law τ, where τ forces q_m to track the virtual control law q_{md}.

Remark 2: In this novel second-order backstepping control (SOBC) design method, we only need one virtual control law q_{md} rather than three virtual control laws in traditional backstepping control design, which effectively reduces the times of differentiation and the possibility of occurring singularity, namely the problem of "explosion of complexity". q_{md} becomes a bridge linking τ and q, as long as τ can force q_m tracking q_{md}, then q_m can force q tracking q_d.

As a consequence, we define two errors

$$e = q - q_d, \tag{3}$$

$$e_m = q_m - q_{md}. \tag{4}$$

And then, we choice ISS for e and e_m during the process of controller design to make e and e_m converge to zero.

$$s = \dot{e} + k_1 e + k_2 \int_0^t e dv, \tag{5}$$

$$s_m = \dot{e}_m + k_1 e_m + k_2 \int_0^t e_m dv, \tag{6}$$

where the gains k_1, k_2 are positive constants. ISS can provide smaller steady-state errors and stronger robustness than LSS.

2.2. Introduction of RBFNN

Since RBFNN can approximate any nonlinear function with any precision in a compact set, it becomes an ideal solution for the issue of unmodeled dynamics.

$$f(x) = W^T h(x) + \varepsilon, \tag{7}$$

where W is the ideal weight matrix, $h(x)$ is the Gaussian basic function vector and ε is the error for approximation that satisfy bounded restriction $|\varepsilon| \leqslant \varepsilon_N$ (ε_N is the upper bound of ε).

Since the nominal mathematical model of the inertia matrix $M(q)$ is relatively easier to acquire, we define $M(q) = M_{no} + \Delta M$, where M_{no} is the nominal part and ΔM denotes the unknown term. In this paper, we utilize two matrices of RBFNN to approximate $C(q,\dot{q})$, $G(q)$, respectively.

Remark 3: Many of papers simply use one RBFNN to approximate a complex term which consists of $C(q,\dot{q})$, $G(q)$. This method will augment burden of the sole RBFNN and in the meantime lower the tracking precision. Nevertheless, the proposed method makes two matrices of RBFNN take the task of approximating $C(q,\dot{q})$ and $G(q)$, which substantially alleviates the burden as well as improves the precision. Moreover, by estimating $C(q,\dot{q})$, $G(q)$ separately, it is easier for researchers to construct different forms of control law and combine RBFNN with other techniques to further improve performance. The two matrices of RBFNN for approximating $C(q,\dot{q})$ and $G(q)$ are designed as follows:

$$\begin{aligned} C_{ij}(q,\dot{q}) &= \sum_{m=1}^{t} \left({W_{Cijm}}^{\mathrm{T}} h_{Cjjm}(q,\dot{q}) \right) + \varepsilon_{Cij} \\ &= {W_{Cij}}^{\mathrm{T}} h_{Cij}(q,\dot{q}) + \varepsilon_{Cij}, \end{aligned} \tag{8}$$

$$\begin{aligned} G_{i1}(q) &= \sum_{m=1}^{t} \left({W_{Gi1m}}^{\mathrm{T}} h_{Gi1m}(q) \right) + \varepsilon_{Gi1} \\ &= {W_{Gi1}}^{\mathrm{T}} h_{Gi1}(q) + \varepsilon_{Gi1}, \end{aligned} \tag{9}$$

where $C_{ij}(q,\dot{q})$, $G_{i1}(q)$ are the elements of $C(q,\dot{q})$, $G(q)$ in ith row and jth column for $i = 1, ..., n$ and $j = 1, ..., n$. t denotes the number of node in RBFNN. Accordingly, the matrices $C(q,\dot{q})$, $G(q)$ can be illustrated as

$$C(q,\dot{q}) = W_C \otimes h_C(q,\dot{q}) + \varepsilon_C(q,\dot{q}), \tag{10}$$

$$G(q) = W_G \otimes h_G(q) + \varepsilon_G(q), \tag{11}$$

where $\otimes$ is a new algorithm we defined in this paper which is represented as follows:

$$W_C \otimes h_C(q) = \begin{bmatrix} W_{C11}^T h_{C11} & \cdots & \cdots & W_{C1n}^T h_{C1n} \\ \cdots & \cdots & \cdots & \cdots \\ \cdots & \cdots & \cdots & \cdots \\ W_{Cn1}^T h_{Cn1} & \cdots & \cdots & W_{Cnn}^T h_{Cnn} \end{bmatrix}, \tag{12}$$

$$W_G \otimes h_G(q) = \begin{bmatrix} W_{G11}^T h_{G11} \\ \cdots \\ \cdots \\ W_{Gn1}^T h_{Gn1} \end{bmatrix}. \tag{13}$$

The ideal RBFNN weights matrices W_C and W_G are comprised of their elements W_{Cij} and W_{Gij} separately; the activation functions matrices h_C and h_G consist of their elements h_{Cij}, h_{Gij} separately; the approximation errors $\varepsilon_C(q,\dot{q})$, $\varepsilon_G(q)$ are composed by the elements ε_{Cij}, ε_{Gi1}, separately.

2.3. Preliminary of DO

Considering the following nonlinear system

$$\dot{h} = f_1(x)u + f_2(x,\dot{x}) + \Delta(t), \tag{14}$$

where $f_1(x)$, $f_2(x,\dot{x})$ are nonlinear functions, u is the input and $\Delta(t)$ denotes the lumped uncertainties of the whole system.

Therefore, DO can be designed in following forms:

$$\begin{aligned} \hat{\Delta}(t) &= p(t) + K_o h, \\ \dot{p}(t) &= -K_o(f_1(x)u + f_2(x,\dot{x}) + \hat{\Delta}(t)), \end{aligned} \tag{15}$$

where K_0 is a positive definite diagonal design matrix, $\hat{\Delta}(t)$ is the estimation of $\Delta(t)$.

2.4. Introduction of needed assumptions

To facilitate design, the assumptions that need to be used are illustrated as follows:

Assumption1: The desired signal q_{id}, ($i = 1, 2, ..., n$) is continuous and available, and $[q_{id}, \dot{q}_{id}, \ddot{q}_{id}]^T \in \Omega_{id}$, ($i = 1, 2, ..., n$) with the known compact set $\Omega_{id} = \{[q_{id}, \dot{q}_{id}, \ddot{q}_{id}]^T : q_{id}^2 + \dot{q}_{id}^2 + \ddot{q}_{id}^2 \leq B_{io}\} \in \mathbb{R}^3$, where B_{io}, ($i = 1, 2, ..., n$) are known positive constants and q_{id}, $\dot{q}_{id}$, $\ddot{q}_{id}$ denotes the ith element of q_d, $\dot{q}_d$, $\ddot{q}_d$.

Assumption2: The time-varying lumped uncertainty is first-order differentiable and its first-order derivative is bounded, i.e., $\tau_{iD}(t)$, ($i = 1, 2, ..., n$) satisfy $|\dot{\tau}_{iD}(t)| \leq \dot{\tau}_{D\max}$ with $\dot{\tau}_{D\max}$ is a positive constant, where $\tau_{iD}(t)$ denotes the ith element of τ_D.

Assumption3: $\Delta M\ddot{q}$ (the matrix uncertainty of $M(q)$) is bounded (it will be formulated in the following text), i.e., $\Delta M\ddot{q}$ satisfy $\|\Delta M\ddot{q}\| < a\|\ddot{q}\| < ap$, where a, p are positive constants and $\|\cdot\|$ denotes the Euclidean norm of a vector.

Remark 4: All the three assumptions are necessary to the stability analysis in Subsection 3.4. $\frac{\|\Delta M\ddot{q}\|^2}{2}$, $\frac{\ddot{q}_{id}^2}{2}$ are the two terms in the polynomial function B_N. If we need to ensure that B_N is bounded, $\frac{\|\Delta M\ddot{q}\|^2}{2}$, $\frac{\ddot{q}_{id}^2}{2}$ must be bounded. Therefore, we need to use Assumptions 1 and 3. $\frac{q_{id}^2}{2}$, $\frac{\dot{q}_{id}^2}{2}$ are the two terms in the polynomial function B_2. If we need to ensure that B_2 is bounded, $\frac{q_{id}^2}{2}$, $\frac{\dot{q}_{id}^2}{2}$ must be bounded. Therefore, we need to use Assumption 1. $\frac{\|\tau_D\|^2}{2}$ is a term in the polynomial function B_D. If we need to ensure that B_D is bounded, $\frac{\|\tau_D\|^2}{2}$ must be bounded. Therefore, we need to use Assumption 2.

3. CONTROL DESIGN

3.1. Preliminary control design

Definition 1 (SGUUB) [22]**:** The solution $x(t)$ of the system is semiglobally uniformly ultimately bounded (SGUUB) if for any compact set Ω and all $x(t_0) \in \Omega$, there exists an $\mu > 0$ and $T(\mu, x(t_0))$ such that $\|x(t)\| \leq \mu$ for all $t > t_0 + T$.

Aiming to achieve the technique of output constraints, BLF [38] is adopted for designing control law. The acquired control law possesses a property that can restrict the movement of FJRM in the limited sphere that we set in advance by adjusting its parameters k_{ai}.

Choose the following symmetric BLF candidate

$$V_1 = \frac{1}{2}\sum_{i=1}^{n} \ln \frac{k_{ai}^2}{k_{ai}^2 - e_i^2}, \tag{16}$$

$$\dot{V}_1 = \sum_{i=1}^{n} \frac{e_i \dot{e}_i}{k_{ai}^2 - e_i^2}, \tag{17}$$

where e_i denotes the ith element of vector e. It is obvious to find that when $|e_i|$ approaches k_{ai}, $\dot{V}_1$ will go to negative infinity to prevent e_i from exceeding k_{ai}. Hence, the output errors are limited in $[-k_{ai}; k_{ai}]$, $i = 1, 2, ..., n$. The specific theory analysis refers to [40].

Thereafter, we add common quadratic lyapunov function terms behind V_1 and generate V_2 (For ease of expression, we use M, C, G, F in the following parts to denote $M(q)$, $C(q,\dot{q})$, $G(q)$, $F(q,\dot{q})$).

$$\begin{aligned} V_2 = {} & V_1 + \frac{1}{2} e_m^T e_m + \frac{1}{2} s^T M s + \frac{1}{2} s_m^T J_m s_m \\ & + \frac{1}{2}(e - e_m)^T K (e - e_m). \end{aligned} \tag{18}$$

Taking the derivative of V_2 with respect to time and take (3), (4), (5), (6) into it, we acquire

$$\begin{aligned} \dot{V}_2 = {} & \sum_{i=1}^{n} \frac{e_i \cdot s_i}{k_{ai}^2 - e_i^2} - \sum_{i=1}^{n} \frac{k_1 e_i^2}{k_{ai}^2 - e_i^2} - \sum_{i=1}^{n} \frac{k_2 e_i \int_0^t e_i dv}{k_{ai}^2 - e_i^2} \\ & + s^T M(\ddot{q} - \ddot{q}_d + k_1 \dot{e} + k_2 e) + s_m^{\mathrm{T}} J_m (\ddot{q}_m - \ddot{q}_{md} \\ & + k_1 \dot{e}_m + k_2 e_m) + (e - e_m)^{\mathrm{T}} K \Bigg(s - k_1 e - s_m \\ & + k_1 e_m - k_2 \int_0^t e dv + k_2 \int_0^t e_m dv \Bigg) + e_m^{\mathrm{T}} (s_m \\ & - k_1 e_m - k_2 \int_0^t e_m dv) + s^T C s. \end{aligned} \tag{19}$$

Transform (19) into

$$\begin{aligned} \dot{V}_2 = {} & - \sum_{i=1}^{n} \frac{k_1 e_i^2}{k_{ai}^2 - e_i^2} - \sum_{i=1}^{n} \frac{k_2 e_i \int_0^t e_i dv}{k_{ai}^2 - e_i^2} - e_m^{\mathrm{T}} k_1 e_m \\ & - e_m^{\mathrm{T}} k_2 \int_0^t e_m dv - (e - e_m)^{\mathrm{T}} K k_1 (e - e_m) \\ & - (e - e_m)^{\mathrm{T}} K k_2 \left(\int_0^t e dv - \int_0^t e_m dv \right) \\ & + s^{\mathrm{T}} \underbrace{(\Psi + M\dot{s} + Cs + K(e - e_m))}_{\text{(A)}} \\ & + s_m^{\mathrm{T}} \underbrace{(e_m + J_m \dot{s}_m - K(e - e_m))}_{\text{(B)}}, \end{aligned} \tag{20}$$

where

$$\Psi = \left[\frac{e_{11}}{k_{a1}^2 - e_{11}^2}, \frac{e_{12}}{k_{a2}^2 - e_{12}^2}, \ldots, \frac{e_{1n}}{k_{an}^2 - e_{1n}^2} \right]^{\mathrm{T}}. \tag{21}$$

Using(1), (3) and (5), (A) in (20) can be transformed into

$$\begin{aligned} (\mathrm{A}) = {} & \Psi - K q_d - F - G - M(\ddot{q}_d - k_1 \dot{e} - k_2 e) \\ & - C \left(\dot{q}_d - k_1 e_1 - k_2 \int_0^t e dv \right) + K q_{md} + \tau_d(t). \end{aligned} \tag{22}$$

Then we define (22) $= -K_1 s$ and acquire the virtual control law q_{md} as follows:

$$\begin{aligned} q_{md} = {} & K^{-1} \Bigg(- K_1 s - \Psi + M(\ddot{q}_d - k_1 \dot{e} - k_2 e) + C \Bigg(\dot{q}_d \\ & - k_1 e - k_2 \int_0^t e dv \Bigg) + F + G - \tau_d(t) \Bigg) + q_d, \end{aligned} \tag{23}$$

where K_1 is a positive definite diagonal matrix that represents the control gain.

And then, using (2), (4) and (6), the term (B) in (20) can be transformed into

$$\begin{aligned} (\mathrm{B}) = {} & e_m + \tau - K(q_{md} - q_d) \\ & - J_m (\ddot{q}_{md} - k_1 \dot{e}_m - k_2 e_m). \end{aligned} \tag{24}$$

Then we define (24) $= -K_2 s_m$ and acquire the actual control law τ as follows:

$$\begin{aligned} \tau = {} & - K_2 s_m - e_m + J_m (\ddot{q}_{md} - k_1 \dot{e}_m - k_2 e_m) \\ & + K(q_{md} - q_d). \end{aligned} \tag{25}$$

As a result, replacing q_{md}, τ in (20) with (23), (25), we obtain

$$\begin{aligned} \dot{V}_2 = {} & - \sum_{i=1}^{n} \frac{k_1 e_i^2}{k_{ai}^2 - e_i^2} - \sum_{i=1}^{n} \frac{k_2 e_i \int_0^t e_i dv}{k_{ai}^2 - e_i^2} - e_m^{\mathrm{T}} k_1 e_m \\ & - e_m^{\mathrm{T}} k_2 \int_0^t e_m dv - (e - e_m)^{\mathrm{T}} K k_1 (e - e_m) \\ & - s^{\mathrm{T}} K_1 s - (e - e_m)^{\mathrm{T}} K k_2 \left(\int_0^t e dv - \int_0^t e_m dv \right) \\ & - s_m^{\mathrm{T}} K_2 s_m. \end{aligned} \tag{26}$$

Proof: Considering the following compact set

$$\Omega = \left\{ \sum_{i=1}^{n} \ln \frac{k_{ai}^2}{k_{ai}^2 - e_i^2} + e_m^T e_m + s^T M s + s_m^T J_m s_m \right.$$

$$+(e-e_m)^T K(e-e_m) \le 2p_1 \Bigg\}. \tag{27}$$

Then

$$\begin{aligned}\dot{V}_2 \le & -\left(k_1-\frac{k_2}{2}\right)\left(\sum_{i=1}^{n}\frac{e_i^2}{k_{ai}^2-e_i^2}+e_m^{\mathrm{T}}e_m+s^{\mathrm{T}}\frac{K_1}{k_1-\frac{k_2}{2}}s\right.\\ & \left.+s_m^{\mathrm{T}}\frac{K_2}{k_1-\frac{k_2}{2}}s_m+(e-e_m)^{\mathrm{T}}K(e-e_m)\right)\\ & +\sum_{i=1}^{n}\frac{k_2\left(\int_0^t e_i dv\right)^2}{2\left(k_{ai}^2-e_i^2\right)}+\int_0^t(e-e_m)^{\mathrm{T}}dvK\frac{k_2}{2}\int_0^t(e\\ & -e_m)\,dv+\frac{k_2}{2}\int_0^t e_m^{\mathrm{T}}dv\int_0^t e_m dv. \end{aligned}\tag{28}$$

If we choose $k_1 > \frac{k_2}{2}$, $\lambda_{\max}(M) \le \lambda_{\min}\left(\frac{K_1}{k_1-\frac{k_2}{2}}\right)$, $\lambda_{\max}(J_m) \le \lambda_{\min}\left(\frac{K_2}{k_1-\frac{k_2}{2}}\right)$, then we can obtain

$$\dot{V}_2 \le -2\left(k_1-\frac{k_2}{2}\right)V_2+Q(t), \tag{29}$$

where

$$\begin{aligned}Q(t)=&\sum_{i=1}^{n}\frac{k_2\left(\int_0^t e_i dv\right)^2}{2\left(k_{ai}^2-e_i^2\right)}+\frac{k_2}{2}\int_0^t e_m^{\mathrm{T}}dv\int_0^t e_m dv\\ &+\int_0^t(e-e_m)^{\mathrm{T}}dvK\frac{k_2}{2}\int_0^t(e-e_m)dv. \end{aligned}\tag{30}$$

According to the compact set Ω, it is obvious that $Q(t)$ is a bounded term and $V_2 \le p_1$. Therefore we define its maximum as $Q_{\max}$. When $V_2 = p_1$,

$$\dot{V}_2 \le -2\left(k_1-\frac{k_2}{2}\right)p_1+Q_{\max}. \tag{31}$$

If we set $\frac{Q_{max}}{2p_1} \le k_1-\frac{k_2}{2}$, then we can obtain $\dot{V}_2 \le 0$. In conclusion, $V_2 \le p_1$ is an invariable set, namely if $V_2(0) \le p_1$, then $V_2(t) \le p_1$ when $t > 0$.

Solving the inequation $\dot{V}_2 \le -2\left(k_1-\frac{k_2}{2}\right)V_2+Q_{\max}$, we obtain

$$\begin{aligned}V_2(t) \le & \frac{Q_{\max}}{2\left(k_1-\frac{k_2}{2}\right)}\\ & +\left(V_2(0)-\frac{Q_{\max}}{2\left(k_1-\frac{k_2}{2}\right)}\right)e^{-2\left(k_1-\frac{k_2}{2}\right)t}. \end{aligned}\tag{32}$$

As a consequence, all of the closed-loop errors of state variables are SGUUB.

Remark 5: The aforementioned virtual control law q_{md} and actual control law τ are preliminary and simplified versions which merely can be used in ideal situation. In practical case, not only are the internal system uncertainties and TVED unknown, but also some state variables, for example $\dot{q}_{md}$ and $\ddot{q}_{md}$, are unmeasurable. Accordingly, in the following parts, we are going to equip q_{md}, τ with RBFNN, DO and first-order filter (FOF) to solve these practical problems and mature the control scheme further.

3.2. Design of first order filter

According to (25), if we intend to obtain τ, we need to know $\dot{q}_{md}$ and $\ddot{q}_{md}$ first. Since we can't measure $\dot{q}_{md}$ and $\ddot{q}_{md}$ directly, we introduce a FOF to estimate them.

The first FOF (FOF1) can be designed as

$$\zeta_1\dot{\hat{q}}_{md}+\hat{q}_{md}=q_{md}, \tag{33}$$

$$\hat{q}_{md}(0)=q_{md}(0), \tag{34}$$

where ζ_1 is a positive constant and $\dot{\hat{q}}_{md}$ is the output of FOF1. We use $\dot{\hat{q}}_{md}$ as the estimation of $\dot{q}_{md}$.

In the same way, the second FOF (FOF2) can be designed as

$$\zeta_2\ddot{\hat{q}}_{md}+\dot{\hat{q}}_{md}=\dot{q}_{md}, \tag{35}$$

$$\dot{\hat{q}}_{md}(0)=\dot{q}_{md}(0), \tag{36}$$

where ζ_2 is a positive constant and $\ddot{\hat{q}}_{md}$ is the output of FOF2. We use $\ddot{\hat{q}}_{md}$ as the estimation of $\ddot{q}_{md}$.

3.3. Design of DNISMCOC

Using $M(q)=M_{no}+\Delta M$, (10), (11), the dynamic model of FJRM ((1), (2)) can be rewritten as

$$\begin{aligned}&M_{no}(q)\ddot{q}+W_C\otimes h_C(q,\dot{q})\dot{q}+W_G\otimes h_G(q)\\ &=K(q_m-q)+\tau_D(t),\\ &J_m\ddot{q}_m+K(q_m-q)=\tau, \end{aligned}\tag{37}$$

where $\tau_D(t)=\tau_d(t)-F(q,\dot{q})-\Delta M\ddot{q}-\varepsilon_C(q,\dot{q})\dot{q}-\varepsilon_G(q)$ is a lumped uncertainty of the system.

Introducing above-mentioned RBFNN in Subsection 2.2 to approximate $W_C\otimes h_C(q,\dot{q})$, $W_G\otimes h_G(q)$, we can define

$$C_{NN}(q,\dot{q})=\hat{W}_C\otimes h_C(q,\dot{q}), \tag{38}$$

$$G_{NN}(q)=\hat{W}_G\otimes h_G(q), \tag{39}$$

where $\hat{W}_C$, $\hat{W}_G$ are the estimations of weights matrices W_C, W_G.

Accordingly, using (37), (38), (39), we can rewrite (23) as

$$\begin{aligned}q_{md}=&K^{-1}\left(-K_1s-\Psi+M_{no}(q)\left(\ddot{q}_d-k_1\dot{e}-k_2e\right)\right.\\ &+C_{NN}(q,\dot{q})\left(\dot{q}_d-k_1e-k_2\int_0^t edv\right)+G_{NN}(q)\\ &\left.-\tau_D\right)+q_d. \end{aligned}\tag{40}$$

And the network updating laws are suggested as

$$\dot{\hat{W}}_{C_{ij}}=\Gamma_{C_{ij}}h_{C_{ij}}(q,\dot{q})\dot{q}_{rj}r_i-\Gamma_{C_{ij}}\eta_C\hat{W}_{C_{ij}}, \tag{41}$$

$$\dot{\hat{W}}_{G_{i1}}=\Gamma_{G_{i1}}h_{G_{i1}}(q)r_i-\Gamma_{G_{i1}}\eta_G\hat{W}_{G_{i1}}, \tag{42}$$

where $i=1, ..., n$ and $j=1, ..., n$ denote the ith row and jth column of $C_{NN}(q,\dot{q})$, $G_{NN}(q)$, respectively. Γ_{Cij}, Γ_{Gi1}

are positive definite diagonal matrices, and $\dot{q}_{rj}$, r_i denote the jth and ith elements of $\dot{q}_r$, r respectively. And r, $\dot{q}_r$ are defined as follows:

$$r = -\dot{e} - \Lambda e, \tag{43}$$

$$\dot{q}_r = \dot{q}_d - \Lambda e, \tag{44}$$

where Λ is a positive constant diagonal matrix.

Then, we introduce above-mentioned DO to approximate the lumped uncertainty τ_D. On the basis of the contents in Subsection 2.3, we start to design DO for $\tau_D(t)$. Transforming (1) into the form that is similar to (14), we obtain

$$\begin{aligned}\ddot{q} = {} & M_{no}(q)^{-1}K(q_m - q) - M_{no}(q)^{-1}C_{NN}(q,\dot{q})\dot{q} \\ & - M_{no}(q)^{-1}G_{NN}(q) + M_{no}(q)^{-1}\tau_D(t),\end{aligned} \tag{45}$$

where comparing with (14), $M_{no}(q)^{-1}\tau_D(t)$ corresponds to $\Delta(t)$, $M_{no}(q)^{-1}$ corresponds to $f(x_1)$, $K(q_m - q)$ corresponds to u, $-M_{no}(q)^{-1}C_{NN}(q,\dot{q})\dot{q} - M_{no}(q)^{-1}G_{NN}(q)$ corresponds to $f_2(x,\dot{x})$, $\dot{q}$ corresponds to h.

Next, the DO can be designed as

$$\hat{\Delta}(t) = p(t) + K_o\dot{q}, \tag{46}$$

$$\begin{aligned}\dot{p}(t) = {} & -K_o\big(M_{no}(q)^{-1}K(q_m - q) \\ & - M_{no}(q)^{-1}C_{NN}(q,\dot{q})\dot{q} \\ & - M_{no}(q)^{-1}G_{NN}(q) + \hat{\Delta}(t)\big),\end{aligned} \tag{47}$$

$$\hat{\tau}_D(t) = M_{no}(q)\hat{\Delta}(t), \tag{48}$$

where $\hat{\tau}_D$ is the estimation of τ_D.

Replacing τ_D in (40) with $\hat{\tau}_D$, the ultimate virtual control law q_{md} can be written as

$$\begin{aligned}q_{md} = {} & K^{-1}\left(-K_1 s - \Psi + M_{no}(q)\left(\ddot{q}_d - k_1\dot{e} - k_2 e\right)\right. \\ & + C_{NN}(q,\dot{q})\left(\dot{q}_d - k_1 e - k_2\int_0^t e dv\right) + G_{NN}(q) \\ & \left. - \hat{\tau}_D\right) + q_d.\end{aligned} \tag{49}$$

Remark 6: This composite control law combines the merits of RBFNN and DO. The estimation errors from RBFNN are observed by DO further. To some extent, the errors are decreased and are smaller than using single RBFNN or DO for approximating in the condition of the same values of control gains.

Replacing $\dot{q}_{md}$, $\ddot{q}_{md}$ with $\dot{\hat{q}}_{md}$, $\ddot{\hat{q}}_{md}$, respectively in (25) and placing (49) in (25), we can obtain

$$\begin{aligned}\tau = {} & -\left(K_2 + J_m k_1\right)\dot{q}_m - \left(K_2 k_1 + I + J_m k_2\right)e_m + \left(K_2\right. \\ & \left. + J_m k_1\right)\dot{\hat{q}}_{md} + J_m\ddot{\hat{q}}_{md} - K_2 k_2\int_0^t e_m dv - K_1 s - \Psi \\ & + M_{no}(q)\left(\ddot{q}_d - k_1\dot{e} - k_2 e\right) + C_{NN}\left(\dot{q}_d - k_1 e\right. \\ & \left. - k_2\int_0^t e dv\right) + G_{NN} - \hat{\tau}_D,\end{aligned} \tag{50}$$

where I denotes a unit matrix. Equation (50) is the ultimate actual control law of DNISMCOC. The whole control process of DNISMCOC is presented in Fig. 2.

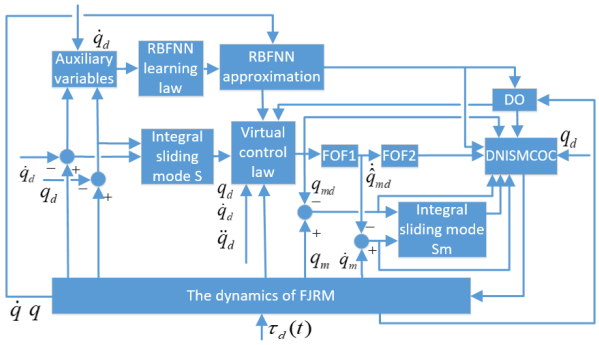

Fig. 2. Block diagram of DNISMCOC.

3.4. System stability analysis

Considering the following compact set

$$\begin{aligned}\Omega_2 = \Bigg\{ & \sum_{i=1}^{n}\ln\frac{k_{ai}^2}{k_{ai}^2 - e_i^2} + e_m^T e_m + s^T M s + s_m^T J_m s_m \\ & + (e - e_m)^T K(e - e_m) + \dot{\tilde{q}}_{md}^T\dot{\tilde{q}}_{md} + \ddot{\tilde{q}}_{md}^T\ddot{\tilde{q}}_{md} \\ & + \tilde{q}_{md}^T\tilde{q}_{md} + r^T M r + \sum_{i=1}^{n}\sum_{j=1}^{n}\tilde{W}_{Cij}^T\Gamma_{Cij}^{-1}\tilde{W}_{Cij} \\ & + \sum_{i=1}^{n}\tilde{W}_{Gi1}^T\Gamma_{Gi1}^{-1}\tilde{W}_{Gi1} + \tilde{\tau}_D^T\tilde{\tau}_D \le 2p_2\Bigg\}.\end{aligned} \tag{51}$$

We design the candidate lyapunov function V_3 as

$$\begin{aligned}V_3 = {} & \frac{1}{2}\sum_{i=1}^{n}\ln\frac{k_{ai}^2}{k_{ai}^2 - e_i^2} + \frac{1}{2}e_m^T e_m \\ & + \frac{1}{2}s^T M s + \frac{1}{2}s_m^T J_m s_m + \frac{1}{2}(e - e_m)^T K(e - e_m) \\ & + \frac{1}{2}\dot{\tilde{q}}_{md}^T\dot{\tilde{q}}_{md} + \frac{1}{2}\ddot{\tilde{q}}_{md}^T\ddot{\tilde{q}}_{md} + \frac{1}{2}\tilde{q}_{md}^T\tilde{q}_{md} + \frac{1}{2}r^T M r \\ & + \frac{1}{2}\sum_{i=1}^{n}\sum_{j=1}^{n}\tilde{W}_{Cij}^T\Gamma_{Cij}^{-1}\tilde{W}_{Cjj} + \frac{1}{2}\sum_{i=1}^{n}\tilde{W}_{Gi1}^T\Gamma_{Gi1}^{-1}\tilde{W}_{Gi1} \\ & + \frac{1}{2}\tilde{\tau}_D^T\tilde{\tau}_D,\end{aligned} \tag{52}$$

where $\tilde{W}_{Cij}$, $\tilde{W}_{Gi1}$ are estimation errors of W_{Cij}, W_{Gi1} which are defined as

$$\begin{aligned}\hat{W}_{Cj} - W_{Cij} &= \tilde{W}_{Cjj}, \\ \hat{W}_{Gi1} - W_{Gi1} &= \tilde{W}_{Gi1}.\end{aligned} \tag{53}$$

$\tilde{\tau}_D$ is the estimation error of the lumped uncertainty τ_D which is defined as $\tilde{\tau}_D = \hat{\tau}_D - \tau_D$. And in (52)

$$\begin{aligned}\tilde{q}_{md} &= \hat{q}_{md} - q_{md}, \\ \dot{\tilde{q}}_{md} &= \dot{\hat{q}}_{md} - \dot{q}_{md}, \\ \ddot{\tilde{q}}_{md} &= \ddot{\hat{q}}_{md} - \ddot{q}_{md}.\end{aligned} \tag{54}$$

Besides

$$V_2 = \frac{1}{2}\sum_{i=1}^{n}\ln\frac{k_{ai}^2}{k_{ai}^2-e_i^2}+\frac{1}{2}e_m^Te_m+\frac{1}{2}s^TMs+\frac{1}{2}s_m^TJ_ms_m + \frac{1}{2}(e-e_m)^TK(e-e_m)+\frac{1}{2}\dot{\tilde{q}}_{md}^T\dot{\tilde{q}}_{md}+\frac{1}{2}\dot{\tilde{q}}_{md}^T\tilde{\tilde{q}}_{md} + \frac{1}{2}\tilde{q}_{md}^T\tilde{q}_{md}, \tag{55}$$

$$V_{NN} = \frac{1}{2}r^TMr+\frac{1}{2}\sum_{i=1}^{n}\sum_{j=1}^{n}\tilde{W}_{Cij}^T\Gamma_{Cij}^{-1}\tilde{W}_{Cij} + \frac{1}{2}\sum_{i=1}^{n}\tilde{W}_{Gil}^T\Gamma_{Gi1}^{-1}\tilde{W}_{Gi1}, \tag{56}$$

$$V_D = \frac{1}{2}\tilde{\tau}_D^T\tilde{\tau}_D. \tag{57}$$

Differentiating V_3 with respect to time, we obtain

$$\begin{aligned}\dot{V}_3 = {} & \dot{V}_2+\dot{V}_{NN}+\dot{V}_D \\ & -\sum_{i=1}^{n}\frac{k_1e_i^2}{k_{ai}^2-e_i^2}-\sum_{i=1}^{n}\frac{k_2e_i\int_0^t e_idv}{k_{ai}^2-e_i^2} \\ & -e_m^{\mathrm{T}}k_1e_m-e_m^{\mathrm{T}}k_2\int_0^t e_mdv-(e-e_m)^{\mathrm{T}}Kk_1(e-e_m) \\ & -(e-e_m)^{\mathrm{T}}Kk_2\left(\int_0^t edv-\int_0^t e_mdv\right)+s^{\mathrm{T}}\Bigg(\Psi \\ & -Kq_d-G-F+\tau_d-M(\ddot{q}_d-k_1\dot{e}-k_2e) \\ & -C\left(\dot{q}_d-k_1e_1-k_2\int_0^t edv\right)+Kq_{md}\Bigg) \\ & +s_m^{\mathrm{T}}(e_m-K(q_{md}-q_d)-J_m(\ddot{q}_{md}-k_1\dot{e}_m-k_2e_m) \\ & +\tau)+\dot{\tilde{q}}_{md}^T\ddot{\tilde{q}}_{md}+\dot{\tilde{\tilde{q}}}_{md}^T\ddot{\tilde{\tilde{q}}}_{md}+\dot{\tilde{q}}_{md}^T\dot{\tilde{q}}_{md}+r^T(M\dot{r}+Cr) \\ & +\sum_{i=1}^{n}\sum_{j=1}^{n}\tilde{W}_{cij}^T\Gamma_{Cy}^{-1}\dot{\hat{W}}_{Cij}+\sum_{i=1}^{n}\tilde{W}_{Gil}^T\Gamma_{Gil}^{-1}\dot{\hat{W}}_{Gi1}+\tilde{\tau}_D^T\dot{\tilde{\tau}}_D.\end{aligned} \tag{58}$$

On the basis of (33) and (35), we have

$$\dot{\tilde{q}}_{md}^T\ddot{\tilde{q}}_{md} = -\frac{\dot{\tilde{q}}_{md}^T\dot{\tilde{q}}_{md}}{\zeta_1}-\dot{\tilde{q}}_{md}^T\ddot{q}_{md}, \tag{59}$$

$$\dot{\tilde{\tilde{q}}}_{md}^T\ddot{\tilde{\tilde{q}}}_{md} = -\frac{1}{\zeta_2}\dot{\tilde{\tilde{q}}}_{md}^T\ddot{\tilde{q}}_{md}+\frac{1}{\zeta_1^2\zeta_2}\dot{\tilde{\tilde{q}}}_{md}^T\tilde{q}_{md}+\frac{1}{\zeta_1\zeta_2}\dot{\tilde{\tilde{q}}}_{md}^T\dot{q}_{md} - \frac{1}{\zeta_2}\dot{\tilde{\tilde{q}}}_{md}^T\ddot{q}_{md}-\dot{\tilde{\tilde{q}}}_{md}^T\dddot{q}_{md}, \tag{60}$$

$$\dot{\tilde{q}}_{md}^T\dot{\tilde{q}}_{md} = -\frac{1}{\zeta_1}\dot{\tilde{q}}_{md}^T\tilde{q}_{md}-\dot{\tilde{q}}_{md}^T\dot{q}_{md}. \tag{61}$$

Taking use of (49), (50) to substitute for q_{md}, τ and placing (59), (60), (61) in (58), we acquire

$$\begin{aligned}\dot{V}_2 = {} & -\sum_{i=1}^{n}\frac{k_1e_i^2}{k_{ai}^2-e_i^2}-\sum_{i=1}^{n}\frac{k_2e_i\int_0^t e_idv}{k_{ai}^2-e_i^2}-e_m^{\mathrm{T}}k_1e_m \\ & -(e-e_m)^{\mathrm{T}}Kk_2\left(\int_0^t edv-\int_0^t e_mdv\right)-s^{\mathrm{T}}K_1s \\ & -e_m^{\mathrm{T}}k_2\int_0^t e_mdv-(e-e_m)^{\mathrm{T}}Kk_1(e-e_m) \\ & -(e-e_m)^{\mathrm{T}}Kk_2\left(\int_0^t edv-\int_0^t e_mdv\right)-s^{\mathrm{T}}K_1s \\ & +s_m^{\mathrm{T}}\left(J_m\dot{\tilde{q}}_{md}+(K_2+J_mk_1)\dot{\tilde{q}}_{md}\right)-\frac{\dot{\tilde{q}}_{md}^T\dot{\tilde{q}}_{md}}{\zeta_1} \\ & -\dot{\tilde{q}}_{md}^T\ddot{q}_{md}-\frac{1}{\zeta_2}\dot{\tilde{q}}_{md}^T\tilde{\tilde{q}}_{md}+\frac{1}{\zeta_1^2\zeta_2}\dot{\tilde{\tilde{q}}}_{md}^T\tilde{q}_{md} \\ & +\frac{1}{\zeta_1\zeta_2}\dot{\tilde{\tilde{q}}}_{md}^T\dot{q}_{md}-\frac{1}{\zeta_2}\dot{\tilde{q}}_{md}^T\ddot{q}_{md}-\dot{\tilde{q}}_{md}^T\dddot{q}_{md} \\ & -\frac{1}{\zeta_1}\tilde{q}_{md}^T\tilde{q}_{md}-\tilde{q}_{md}^T\dot{q}_{md},\end{aligned} \tag{62}$$

where

$$\begin{aligned}\sigma_C &= C-C_{NN} = \varepsilon_C-\tilde{W}_C\otimes h_C, \\ \sigma_G &= G-G_{NN} = \varepsilon_G-\tilde{W}_G\otimes h_G.\end{aligned} \tag{63}$$

Placing (63) into (62), we can acquire

$$\begin{aligned}\dot{V}_2 = {} & -\sum_{i=1}^{n}\frac{k_1e_i^2}{k_{ai}^2-e_i^2}-\sum_{i=1}^{n}\frac{k_2e_i\int_0^t e_idv}{k_{ai}^2-e_i^2}-e_m^{\mathrm{T}}k_2\int_0^t e_mdv \\ & -e_m^{\mathrm{T}}k_1e_m-(e-e_m)^{\mathrm{T}}Kk_1(e-e_m)-s^{\mathrm{T}}K_1s-(e \\ & -e_m)^{\mathrm{T}}Kk_2\left(\int_0^t edv-\int_0^t e_mdv\right)-s_m^{\mathrm{T}}K_2s_m \\ & +s^{\mathrm{T}}\Delta M(\ddot{e}+k_1\dot{e}+k_2e)+s^{\mathrm{T}}\sigma_C(\dot{e}+k_1e \\ & +k_2\int_0^t edv\Big)+s^{\mathrm{T}}\tilde{W}_C\otimes h_C\dot{q}+s^{\mathrm{T}}\tilde{W}_G\otimes h_G \\ & -s^{\mathrm{T}}\tilde{\tau}_D+s_m^{\mathrm{T}}\left((K_2+J_mk_1)\dot{\tilde{q}}_{md}+J_m\dot{\tilde{\tilde{q}}}_{md}\right) \\ & -\frac{\dot{\tilde{q}}_{md}^T\dot{\tilde{q}}_{md}}{\zeta_1}-\dot{\tilde{q}}_{md}^T\ddot{q}_{md}-\frac{1}{\zeta_2}\dot{\tilde{q}}_{md}^T\tilde{\tilde{q}}_{md}+\frac{1}{\zeta_1^2\zeta_2}\dot{\tilde{\tilde{q}}}_{md}^T\tilde{q}_{md} \\ & +\frac{1}{\zeta_1\zeta_2}\dot{\tilde{\tilde{q}}}_{md}^T\dot{q}_{md}-\frac{1}{\zeta_2}\dot{\tilde{q}}_{md}^T\ddot{q}_{md}-\dot{\tilde{q}}_{md}^T\dddot{q}_{md} \\ & -\frac{1}{\zeta_1}\tilde{q}_{md}^T\tilde{q}_{md}-\tilde{q}_{md}^T\dot{q}_{md}.\end{aligned} \tag{64}$$

Using young's inequality, we obtain

$$\begin{aligned}\dot{V}_2 \le {} & -\left(k_1-\frac{k_2}{2}\right)\Bigg(\sum_{i=1}^{n}\frac{e_i^2}{k_{ai}^2-e_i^2}+e_m^{\mathrm{T}}e_m+(e \\ & -e_m)^{\mathrm{T}}K(e-e_m)+s_m^{\mathrm{T}}\left(\frac{K_2-J_m-J_mk_1-I}{2k_1-k_2}\right)s_m \\ & +\dot{\tilde{\tilde{q}}}_{md}^T\left(\frac{\frac{I}{2\zeta_2}-\frac{I}{2\zeta_1^2\zeta_2}-\frac{I}{2\zeta_1\zeta_2}-\frac{I}{2}-\frac{J_m}{2}}{k_1-\frac{k_2}{2}}\right)\dot{\tilde{\tilde{q}}}_{md} \\ & +s^{\mathrm{T}}\left(\frac{K_1-\frac{5}{2}I}{k_1-\frac{k_2}{2}}\right)s+\left(\frac{\frac{1}{\zeta_1}-\frac{1}{2\zeta_1^2\zeta_2}-\frac{1}{2}}{k_1-\frac{k_2}{2}}\right)\tilde{q}_{md}^T\tilde{q}_{md} \\ & +\dot{\tilde{q}}_{md}^T\left(\frac{\frac{I}{\zeta_1}-\frac{I}{2}-\frac{J_mk_1+K_2}{2}}{k_1-\frac{k_2}{2}}\right)\dot{\tilde{q}}_{md}\Bigg)+B_2.\end{aligned} \tag{65}$$

B_2 is a continuous bounded function which satisfies $|B_2|\le N_2$ (N_2 is a positive constant).

If we set

$$\begin{aligned}&\lambda_{\min}(K_2-J_m-k_1J_m-I)\ge(2k_1-k_2)\lambda_{\max}(J_m), \\ &\lambda_{\min}\left(K_1-\frac{5}{2}I\right)\ge\left(k_1-\frac{k_2}{2}\right)\lambda_{\max}(M),\end{aligned}$$

$$\frac{1}{\zeta_1}-\frac{1}{2\zeta_1^2\zeta_2}-\frac{1}{2}\geq k_1-\frac{k_2}{2},\ k_1>\frac{k_2}{2},$$
$$\lambda_{\min}\left(\frac{I}{2\zeta_2}-\frac{I}{2\zeta_1^2\zeta_2}-\frac{I}{2\zeta_1\zeta_2}-\frac{I}{2}-\frac{J_m}{2}\right)\geq\left(k_1-\frac{k_2}{2}\right)I,$$
$$\lambda_{\min}\left(\frac{I}{\zeta_1}-\frac{I}{2}-\frac{J_mk_1+K_2}{2}\right)\geq\left(k_1-\frac{k_2}{2}\right)I,$$

then we can acquire

$$\dot{V}_2\leq-(2k_1-k_2)V_2+N_2. \tag{66}$$

Placing network updating laws (41), (42) into (58), we acquire

$$\begin{aligned}\dot{V}_{NN}=&\,\mathrm{r}^T(M\dot{r}+Cr)\\&+\sum_{i=1}^{n}\sum_{j=1}^{n}\left(\tilde{W}_{Cij}^Th_{Cij}(q,\dot{q})\dot{q}_{rj}r_i-\tilde{W}_{Cij}^T\eta_C\hat{W}_{Cij}\right)\\&+\sum_{i=1}^{n}\left(\tilde{W}_{Gi1}^Th_{Gi1}(q)r_i-\tilde{W}_{Gi1}^T\eta_G\hat{W}_{Gi1}\right).\end{aligned} \tag{67}$$

On the basis of (43) and (44), (1) can be transformed into

$$\begin{aligned}&M(q)(\ddot{q}_r-\dot{r})+C(q,\dot{q})(\dot{q}_r-r)+G(q)+F(q,\dot{q})\\&=K(q_{md}+e_m-q_d-e)+\tau_d(t).\end{aligned} \tag{68}$$

Placing (10), (11), (38), (39), (49) into (68) and transforming (68) further, we have

$$\begin{aligned}M\dot{r}+Cr=&-\Delta M\ddot{e}-\Delta M\Lambda\dot{e}-\varepsilon_C\dot{e}-\varepsilon_C\Lambda e+K_1s+\Psi\\&-\tilde{W}_C\otimes h_C(q,\dot{q})\dot{q}_r-\tilde{W}_G\otimes h_G(q)-M_{no}(\Lambda\dot{e}\\&-k_1\dot{e}-k_2e)-C_{NN}\left(\Lambda e-k_1e-k_2\int_0^t edv\right)\\&-K(e_m-e)+\tilde{\tau}_D.\end{aligned} \tag{69}$$

Placing (69) into (67) and using the following equations

$$\mathrm{r}^T\tilde{W}_C\otimes h_C(q,\dot{q})\dot{q}_r=\sum_{i=1}^{n}\sum_{j=1}^{n}\tilde{W}_{Cij}^Th_{Cij}(q,\dot{q})\dot{q}_{rj}r_i,$$
$$\mathrm{r}^T\tilde{W}_G\otimes h_G(q)=\sum_{i=1}^{n}\tilde{W}_{Gi1}^Th_{Gi1}(q)r_i,$$

we obtain

$$\begin{aligned}\dot{V}_{NN}=&-r^TM(k_1I-\Lambda)r-r^TMk_1\Lambda e+r^T(M\Lambda^2\\&+k_2M)e+r^T\Delta M(\Lambda\dot{e}-k_1\dot{e}-k_2e)-r^TK(e_m\\&-e)+r^TK_1s-r^T\Delta M\ddot{e}-r^T(\Delta M\Lambda+\varepsilon_C)\dot{e}\\&-r^T(C-\sigma_C)\left(\Lambda e-k_1e-k_2\int_0^t edv\right)\\&-r^T\varepsilon_C\Lambda e+r^T\Psi+r^T\tilde{\tau}_D-\sum_{i=1}^{n}\sum_{j=1}^{n}\tilde{W}_{Cij}^T\eta_C\hat{W}_{Cij}\\&-\sum_{i=1}^{n}\tilde{W}_{Gi1}^T\eta_G\hat{W}_{Gi1}.\end{aligned} \tag{70}$$

Using young's inequation and $2\tilde{W}^T\hat{W}\geq\|\tilde{W}\|^2-\|W\|^2$, we obtain

$$\begin{aligned}\dot{V}_{NN}\leq&-r^T\left(M\left(k_1I-\Lambda-\frac{k_1\Lambda}{2}-\frac{\Lambda^2+k_2I}{2}\right)-4I\right.\\&\left.-\frac{K}{2}-\frac{K_1}{2}\right)\mathrm{r}-\sum_{i=1}^{n}\sum_{j=1}^{n}\frac{\eta_C}{2}\tilde{W}_{Cij}^T\tilde{W}_{Cij}\\&-\sum_{i=1}^{n}\frac{\eta_G}{2}\tilde{W}_{Gi1}^T\tilde{W}_{Gi1}+\sum_{i=1}^{n}\sum_{j=1}^{n}\frac{\eta_C}{2}\|W_{Cij}\|^2\\&+\sum_{i=1}^{n}\frac{\eta_G}{2}\|W_{Gi1}\|^2+\frac{\dot{e}^T\Delta M^T\Delta M\ddot{e}}{2}\\&+(\Lambda\dot{e}-k_1\dot{e}-k_2e)^T\frac{\Delta M^T\Delta M}{2}(\Lambda\dot{e}-k_1\dot{e}-k_2e)\\&+(e_m-e)^T\frac{K}{2}(e_m-e)+s^T\frac{K_1}{2}s+\frac{\varepsilon_G^T\varepsilon_G}{2}+\frac{\Psi^T\Psi}{2}\\&+\left(\Lambda e-k_1e-k_2\int_0^t edv\right)^T\left(\frac{C^TC+\sigma_C^T\sigma_C}{2}\right)\\&\times\left(\Lambda e-k_1e-k_2\int_0^t edv\right)+\frac{e^T\Lambda\varepsilon_C^T\varepsilon_C\Lambda e}{2}\\&+\frac{\tilde{\tau}_D^T\tilde{\tau}_D}{2}+\frac{\dot{e}^T(\Delta M\Lambda+\varepsilon_C)^T(\Delta M\Lambda+\varepsilon_C)\dot{e}}{2}\\&+e^T\frac{M(\Lambda^2+k_1\Lambda+k_2I)}{2}e.\end{aligned} \tag{71}$$

If we set $\lambda_{\min}\left(M\left(k_1I-\Lambda-\frac{k_1\Lambda}{2}-\frac{\Lambda^2+k_2I}{2}\right)-4I-\frac{K}{2}-\frac{K_1}{2}\right)\geq\lambda_{\max}(M)$, $\frac{\eta_C}{2}\geq\lambda_{\max}(\Gamma_{Cij}^{-1})$, $\frac{\eta_G}{2}\geq\lambda_{\max}\left(\Gamma_{Gi1}^{-1}\right)$, then we can acquire

$$\dot{V}_{NN}\leq-V_{NN}+B_N. \tag{72}$$

B_N is a continuous bounded function which satisfies $|B_N|\leq N_N$ (N_N is a positive constant). Then we have

$$\dot{V}_{NN}\leq-V_{NN}+N_N. \tag{73}$$

According to (58)

$$\dot{V}_D=\tilde{\tau}_D^T\dot{\tilde{\tau}}_D=\tilde{\tau}_D^T\left(\dot{\hat{\tau}}_D-\dot{\tau}_D\right). \tag{74}$$

Differentiating (48) once, we have

$$\dot{\hat{\tau}}_D=\dot{M}_{no}(q)\hat{\Delta}(t)+M_{no}(q)\dot{\hat{\Delta}}(t). \tag{75}$$

Differentiating (46) once, we have

$$\dot{\hat{\Delta}}(t)=\dot{p}(t)+K_o\ddot{q}. \tag{76}$$

Placing (76), (47) into (75) and using (37), we obtain

$$\begin{aligned}\dot{\hat{\tau}}_D=&\dot{M}_{no}(q)\hat{\Delta}(t)-K_o\tilde{\tau}_D+K_o\tilde{W}_C\otimes h_C(q,\dot{q})\dot{q}\\&+K_o\tilde{W}_G\otimes h_G(q).\end{aligned} \tag{77}$$

Placing (77) into (74), we have

$$\begin{aligned}\dot{V}_D=&\tilde{\tau}_D^TK_o\tilde{\tau}_D+\tilde{\tau}_D^T\dot{M}_{no}(q)\hat{\Delta}(t)+\tilde{\tau}_D^TK_o\tilde{W}_C\otimes h_C(q,\dot{q})\dot{q}\\&+\tilde{\tau}_D^TK_o\tilde{W}_G\otimes h_G(q)-\tilde{\tau}_D^T\dot{\tau}_D.\end{aligned} \tag{78}$$

Using young's inequation, we have

$$\dot{V}_D\leq-\tilde{\tau}_D^T\left(\frac{K_o}{2}-I\right)\tilde{\tau}_D+B_D. \tag{79}$$

B_D is a continuous bounded function which satisfies $|B_D|\leq N_D$ (N_D is a positive constant).

Then we can obtain

$$\dot{V}_D\leq-\lambda_{\min}(K_o-2I)V_D+N_D. \tag{80}$$

To sum up,

$$\dot{V}_3\leq-\vartheta V_3+N, \tag{81}$$

where $\vartheta=\min(2k_1-k_2,1,\lambda_{\min}(K_o-2I))$, $N=N_2+N_N+N_D$.

According to the compact set Ω_2, we can conclude that $V_3 \leq p_2$. When $V_3 = p_2$,

$$\dot{V}_3 \leq -\vartheta p_2 + N. \tag{82}$$

If we set $2k_1 > k_2$, $\lambda_{\min}(K_o) > 2$, $\frac{N}{p_2} \leq \vartheta$, then we can obtain $\dot{V}_3 \leq 0$. In conclusion, $V_3 \leq p_2$ is an invariable set ,namely, if $V_3(0) \leq p_2$, then $V_3(t) \leq p_2$ when $t > 0$. Solving the inequality (82), we have

$$V_3 \leq \frac{N}{\vartheta} + \left(V_3(0) - \frac{N}{\vartheta}\right) e^{-\vartheta t}. \tag{83}$$

Therefore, we can conclude that all of the closed-loop errors of state variables are SGUUB and the system can realize stability.

4. SIMULATION STUDIES

In this section, the effectiveness of DNISMCOC will be verified through the following several comparisons. **I:** compare with LSS [28] in FJRM control for demonstrating the superiority of ISS for finite-time convergence and reduction of steady-state errors. **II:** compare with traditional forth-order backstepping dynamic surface control (DSC) [26] for showing the superiority of SOBC in reduction of tracking errors and singularity avoidance. **III:** compare with NN-based controller (NNC) [15] and NN-TSMD controller [22], the superiority of DO proposed in this paper can be proved. **IV:** compare with single RBFNN controller (SNNC) [14] for showing the excellence of the proposed method in tracking precision. Besides, two simulation comparisons about parameter setting are shown in **V** and **VI**. In **V**, we maintain the parameters of RBFNN invariable (same as the parameter values in **I**, **II**, **III**, **IV**) and lower the values of all the gains including the gains of DO twice to see how their changes in each times affect the performance of our algorithm. In **VI**, we maintain the values of all the gains invariable (same as the parameter values in **I**, **II**, **III**, **IV**) and change the values of parameters of RBFNN twice to see how their changes in each times affect the performance of our algorithm. The parameter combinations for the two variations in **V** and **VI** are shown in Tables 1 and 2, respectively. Without loss of generality, a two-link FJRM is used for the following simulations. The dynamic of the FJRM in (1), (2) is described by

$$M(q) = \begin{bmatrix} (m_1+m_2)l_1^2 + m_2 l_2^2 + 2m_2 l_1 l_2 \cos(q_2) + J_1 & m_2 l_2^2 + m_2 l_1 l_2 \cos(q_2) \\ m_2 l_2^2 + m_2 l_1 l_2 \cos(q_2) & m_2 l_2^2 + J_2 \end{bmatrix},$$

$$C(q,\dot{q}) = \begin{bmatrix} -m_2 l_1 l_2 \sin(q_2)\dot{q}_2 & -m_2 l_1 l_2 \sin(q_2)\dot{q}_1 - m_2 l_1 l_2 \sin(q_2)\dot{q}_2 \\ m_2 l_1 l_2 \sin(q_2)\dot{q}_1 & 0 \end{bmatrix},$$

$$G(q) = \begin{bmatrix} (m_1+m_2) l_1 g \cos q_1 + m_2 l_2 g \cos(q_1+q_2) \\ m_2 l_2 g \cos(q_1+q_2) \end{bmatrix},$$

$$F(\dot{q}) = 0.2\,\mathrm{sign}(\dot{q}),\ K = \begin{bmatrix} 400 & 0 \\ 0 & 400 \end{bmatrix},\ J_m = \begin{bmatrix} 1 & 0 \\ 0 & 1 \end{bmatrix},$$

Table 1. The parameter setting in comparison **V**.

Parameter	Original setting	First resetting	Second resetting
K_1	500	450	400
K_2	500	450	400
k_1	35	30	25
k_2	20	15	10
K_0	500	450	400

Table 2. The parameter setting in comparison **VI**.

Parameter	Original setting	First resetting	Second resetting
b	10	5	1
$\Gamma_{Cij} = \Gamma_{Gi1}$	100	75	50
$\eta_{Cij} = \eta_{Gi1}$	0.0001	0.0005	0.001
Λ	50	40	30

where q_1, q_2 stand for the angle positions of the two joints, and $\dot{q}_1$, $\dot{q}_2$ are angle velocities of the two joints. The nominal parameters for the system are selected as $l_1^0 = 1$ m, $l_2^0 = 0.8$ m, $\mathrm{m}_1^0 = 0.5$ kg, $\mathrm{m}_2^0 = 1.5$ kg, $\mathrm{J}_1^0 = 5\ \mathrm{kg}\cdot\mathrm{m}^2$, $\mathrm{J}_2^0 = 5\ \mathrm{kg}\cdot\mathrm{m}^2$. The gravitational acceleration g is 9.8 kg/N. Initial conditions of simulations are given as $q(0) = [0.02, 0.02]^T$, $\dot{q}(0) = [0.001, 0.001]^T$, $q_m(0) = [0.001, 0.001]^T$, $\dot{q}_m(0) = [0.001, 0.001]^T$. The desired trajectories q_1, q_2 are given as $q_{1d} = 0.3\sin(2t)$, $q_{2d} = 0.3\sin(2t)$. TVED are given as $\tau_{d1} = 2\sin t + 0.5\sin(200t)$, $\tau_{d2} = \cos 2t + 0.5\sin(200t)$. In view of system uncertainties, an additive variance of 20% of their nominal values is considered for practical value, which implies $m_1 = \mathrm{m}_1^0 + 0.2\ \mathrm{m}_1^0, m_2 = \mathrm{m}_2^0 + 0.2\ \mathrm{m}_2^0$, $\mathrm{J}_1 = \mathrm{J}_1^0 + 0.2\ \mathrm{J}_1^0$, $\mathrm{J}_2 = \mathrm{J}_2^0 + 0.2\ \mathrm{J}_2^0$. The control gains of DNISMCOC are chosen as $K_1 = \begin{bmatrix} 500 & 0 \\ 0 & 500 \end{bmatrix}$, $K_2 = \begin{bmatrix} 500 & 0 \\ 0 & 500 \end{bmatrix}$. The parameters of ISS are selected as $k_1 = 35$, $k_2 = 20$. The parameters of BLV are selected as $k_{a1} = 0.1$, $k_{a2} = 0.1$. With regard to RBFNN, we chose eleven-nodes RBFNN to estimate each element of $C(q,\dot{q})$ and $G(q)$. The center of the Gaussian function is selected as $\mu_{ij} \in (-0.3, 0.3)$, and the scaling parameter is chosen as $b_{Cij} = 10$, $b_{Gi1} = 10$. The values of adaptive gains in (41), (42) are taken to be $\Gamma_{C_{ij}} = 100$, $\Gamma_{G_{i1}} = 100$, $\eta_{C_{ij}} = 0.0001$, $\eta_{G_{i1}} = 0.0001$, $\Lambda = \begin{bmatrix} 50 & 0 \\ 0 & 50 \end{bmatrix}$. The parameters of DO are set as $K_o = \begin{bmatrix} 500 & 0 \\ 0 & 500 \end{bmatrix}$, and the parameters of FOF1, FOF2 are set as $\zeta_1 = 0.0001, \zeta_2 = 0.0001$. The position tracking results of the two joints are shown in Figs. 3 and 4.

I: Comparison between LSS and the designed ISS of DNISMCOC in FJRM control.

To facilitate the comparisons, the backstepping control gains in LSS will be chosen same as in DNISMCOC. Ac-

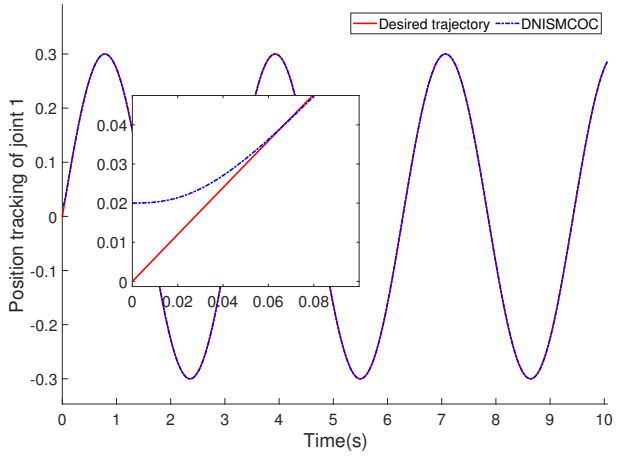

Fig. 3. Position tracking of joint 1.

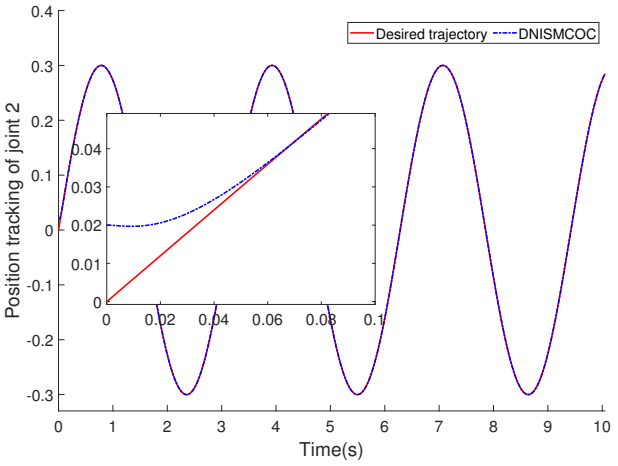

Fig. 4. Position tracking of joint 2.

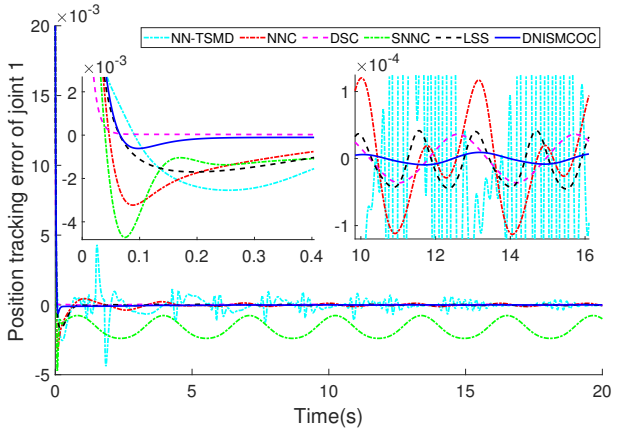

Fig. 5. Position tracking error of joint 1.

cording to Figs. 5-8, we can see that DNISMCOC provides superior tracking performance for the FJRM system even in presence of system uncertainties and TVED. Besides, in the condition of the same control gains, ISS of

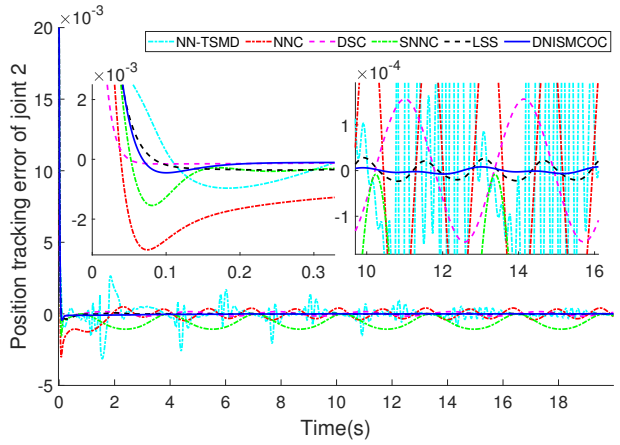

Fig. 6. Position tracking error of joint 2.

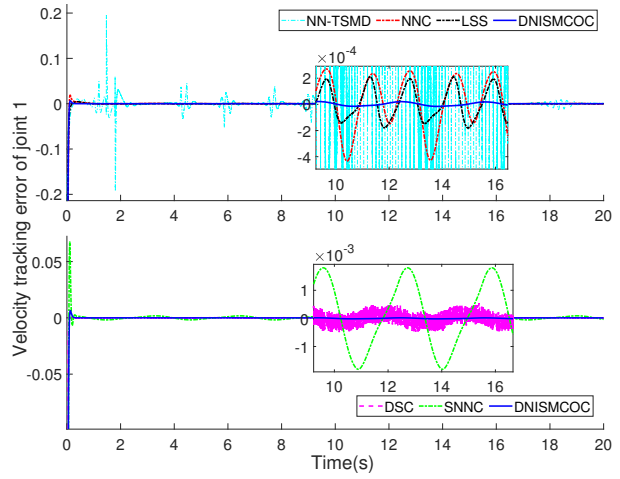

Fig. 7. Velocity tracking error of joint 1.

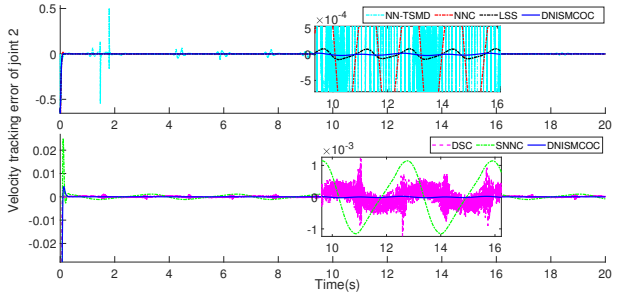

Fig. 8. Velocity tracking error of joint 1.

DNISMCOC provides faster speed on convergence and lower steady-state errors than LSS both in tracking of positions and velocities. All these advantages are owing to the integral term in ISS.

II: Comparison between DSC and DNISMCOC.

The simulation results are shown as Figs. 5-10. According to Figs. 5-8, we can learn that both DSC and DNISMCOC can offer great tracking performance, yet DNISM-

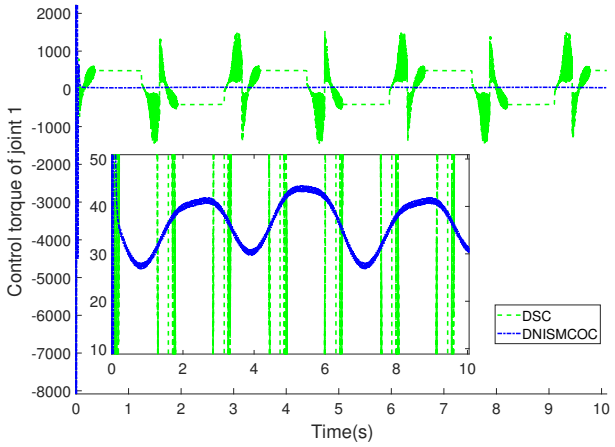

Fig. 9. Control torque of joint 1.

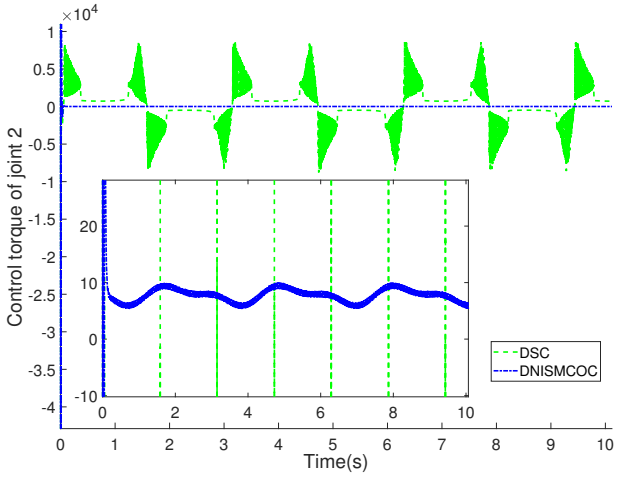

Fig. 10. Control torque of joint 2.

COC offers lower steady-state errors in the tracking of positions and velocities and there are high frequency jumps in velocity tracking errors of DSC. Furthermore, from the torque results in Figs. 9 and 10, it is inevitable in singularity for DSC because of its multiple differentiation, which can be clearly observed through its periodic jumps in torque. Nevertheless, the torques of DNISMCOC in joints 1 and 2 are periodically smooth curves, which significantly proves its effectiveness in singularity avoidance.

III: Comparison among NNC, NN-TSMD and DNISMCOC.

From the tracking error results in Figs. 5-8, it is obvious that there are periodically sudden jumps in the results of NN-TSMD during the tracking process, and in the process of velocity tracking, this phenomenon is more pronounced. The reason is the complexity of TSMD and its introduction of fraction-order term in mathematical equations. Therefore, the superiority of DO for its simplicity is revealed. As to NNC, we can find that its steady-state

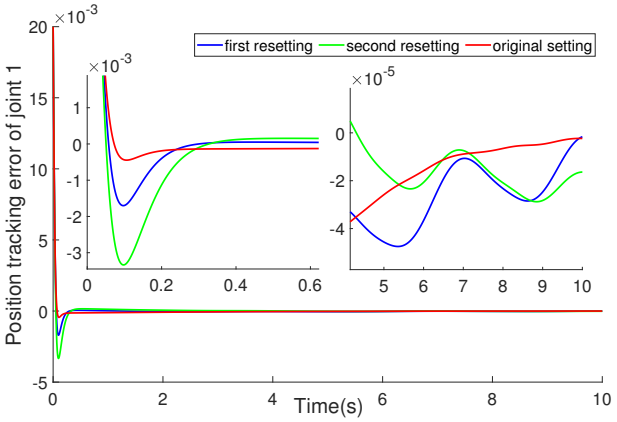

Fig. 11. Position tracking error of joint 1 in **V**.

errors of positions and velocities are larger than DNISMCOC. This is because NNC only uses NN for approximation and not in combination with DO for approximation.

IV: Comparison between SNNC and DNISMCOC.

On the basis of the simulation results shown in Figs. 5-8, we can see that the position tracking results of SNNC can't be regarded as truly successful tracking, for its position tracking errors in both joint 1 and joint 2 still locating below the zero point from start to finish rather than periodically crossing it. This is because SNNC only uses one RBFNN to approximate a complex term in the control law, and its tracking performance is naturally not as good as DNISMCOC, which uses two RBFNN matrices to separately approximate the two uncertain matrices in the control law.

V: How the changes of the values of the gains affect the performance of our algorithm.

Fig. 11 shows the simulation results of this comparison. In accordance with Fig. 11, we can see that the position tracking errors of the three parameter setting schemes remain the same order of magnitude for all gain values reduced twice. However, based on the enlarged plot in Fig. 11, we can find that the higher the values of gains are, the lower the steady-state errors are and the faster the convergence rate is.

VI: How the changes of the values of parameters of RBFNN affect the performance of our algorithm.

Fig. 12 shows the simulation results of this comparison. According to Fig. 12, we can learn that the effect of parameter changes of RBFNN on simulation results is not significant. This is because the curves of the three sets of parameters largely overlap in the case of order of 10^{-4}. This phenomenon demonstrates the strong robustness of RBFNN to parameter changes. Nevertheless, from the enlarged plot in Fig. 12, we can still see that "original setting" has the best simulation results for its smoother curve. Therefore, we can conclude that smaller η_{Cij}, η_{Gi1} and

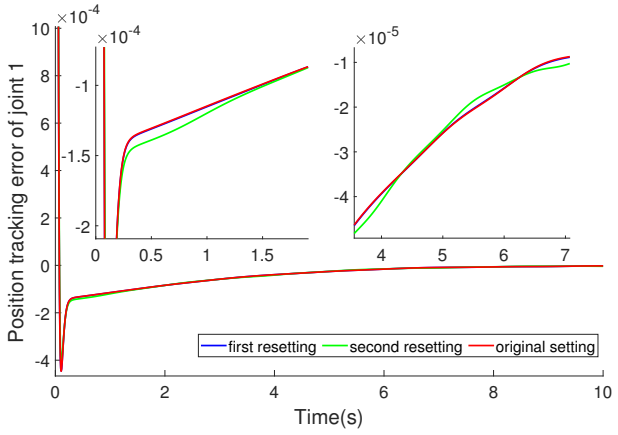

Fig. 12. Position tracking error of joint 1 in **VI**.

larger b, Γ_{Cij}, Γ_{Gi1}, Λ provide relatively better tracking results.

5. CONCLUSION

This paper puts forward a novel DNISMCOC for FJRM in the presence of the system uncertainties and TVED. Specifically, DNISMCOC uses RBFNN to estimate the internal uncertainties of the system, uses DO to estimate TVED and compensate for the estimation errors of RBFNN, uses BLF to limit the error range of the control outputs to ensure safety in practical use. Different from the traditional RBFNN control schemes, DNISMCOC uses multiple RBFNNs to approximate each element of the uncertain matrices of FJRM dynamic. Besides, a DO is introduced for approximating the lumped disturbances which consist of errors of RBFNN, TVED, friction term and system uncertainties of parameters. This method combines the merits of both RBFNN and DO. Moreover, ISS is introduced to reduce steady-state errors and speed up convergence. Since the problem of "explosion of complexity" is a commonly happened difficulty in backstepping control design, we propose a new backstepping design method for FJRM with output constraint which effectively decreases the times of differentiation and alleviates the problem of "explosion of complexity". In addition, we achieve output constraints by employing BLF. Through the lyapunov stability analysis, we identify that the proposed controller can guarantee stability. In the end, simulations are conducted, and the results verify the effectiveness of the proposed control scheme.

In the future research, we will consider to design the controller based on the dynamic model of electrically driven FJRM which takes the dynamic of DC motor into consideration. In addition, force tracking for robotic manipulator is also a promising technology we planned to realize in the future study.

REFERENCES

[1] D. S. Naidu, "Singular perturbation analysis of a flexible beam used in underwater exploration," *International Journal of Systems Science*, vol. 42, no. 1, pp. 183-194, 2011.

[2] N. D. Phu, V. Putov, and C. T. Su, "Mathematical models and adaptive control system of rigid and flexible 4-dof joint robotic manipulator with executive electric drives," in Proc. of International Conference on Control in Technical Systems (CTS), IEEE, pp. 285-289, 2019.

[3] K. Nanos and E. G. Papadopoulos, "On the dynamics and control of flexible joint space manipulators," *Control Engineering Practice*, vol. 45, pp. 230-243, 2015.

[4] J. Nubert, J. Köhler, V. Berenz, F. Allgöwer, and S. Trimpe, "Safe and fast tracking on a robot manipulator: Robust mpc and neural network control," *IEEE Robotics and Automation Letters*, vol. 5, no. 2, pp. 3050-3057, 2020.

[5] W. Zhang, X. Yang, Z. Xu, W. Zhang, L. Yang, and X. Liu, "An adaptive fault-tolerant control method for robot manipulators," *International Journal of Control, Automation, and Systems*, pp. 1-13, 2021.

[6] A. De Luca, A. Albu-Schaffer, S. Haddadin, and G. Hirzinger, "Collision detection and safe reaction with the dlr-iii lightweight manipulator arm," *Proc. of IEEE/RSJ International Conference on Intelligent Robots and Systems*, IEEE, pp. 1623-1630, 2006.

[7] X. Liu, C. Yang, Z. Chen, M. Wang, and C.-Y. Su, "Neuro-adaptive observer based control of flexible joint robot," *Neurocomputing*, vol. 275, pp. 73-82, 2018.

[8] M.-C. Chien and A.-C. Huang, "Adaptive control for flexible-joint electrically driven robot with time-varying uncertainties," *IEEE Transactions on Industrial Electronics*, vol. 54, no. 2, pp. 1032-1038, 2007.

[9] Y. Yang, J. Li, C. Hua, and X. Guan, "Adaptive synchronization control design for flexible telerobotics with actuator fault and input saturation," *International Journal of Robust and Nonlinear Control*, vol. 28, no. 3, pp. 1016-1034, 2018.

[10] C. Yang, T. Teng, B. Xu, Z. Li, J. Na, and C.-Y. Su, "Global adaptive tracking control of robot manipulators using neural networks with finite-time learning convergence," *International Journal of Control, Automation, and Systems*, vol. 15, no. 4, pp. 1916-1924, 2017.

[11] C. Wang, X. Chen, J. Cao, J. Qiu, Y. Liu, and Y. Luo, "Neural network-based distributed adaptive pre-assigned finite-time consensus of multiple TCP/AQM networks," *IEEE Transactions on Circuits and Systems I: Regular Papers*, vol. 68, no. 1, pp. 387-395, 2020.

[12] D. Cui, Y. Wu, and Z. Xiang, "Finite-time adaptive fault-tolerant tracking control for nonlinear switched systems with dynamic uncertainties," *International Journal of Robust and Nonlinear Control*, vol. 31, no. 8, pp. 2976-2992, 2021.

[13] L. Ma, N. Xu, X. Zhao, G. Zong, and X. Huo, "Small-gain technique-based adaptive neural output-feedback fault-tolerant control of switched nonlinear systems with unmodeled dynamics," *IEEE Transactions on Systems, Man,*

and Cybernetics: Systems, vol. 51, no. 11, pp. 7051-7062, 2020.

[14] W. He, Z. Yan, Y. Sun, Y. Ou, and C. Sun, "Neural-learning-based control for a constrained robotic manipulator with flexible joints," *IEEE transactions on neural networks and learning systems*, vol. 29, no. 12, pp. 5993-6003, 2018.

[15] Z. Chen, X. Yang, and X. Liu, "RBFNN-based nonsingular fast terminal sliding mode control for robotic manipulators including actuator dynamics," *Neurocomputing*, vol. 362, pp. 72-82, 2019.

[16] T. Sun, L. Cheng, W. Wang, and Y. Pan, "Semiglobal exponential control of Euler-Lagrange systems using a sliding-mode disturbance observer," *Automatica*, vol. 112, 108677, 2020.

[17] Q. Hou, S. Ding, and X. Yu, "Composite super-twisting sliding mode control design for pmsm speed regulation problem based on a novel disturbance observer," *IEEE Transactions on Energy Conversion*, vol. 36, no. 4, pp. 2591-2599, 2021.

[18] S. Ding, W.-H. Chen, K. Mei, and D. J. Murray-Smith, "Disturbance observer design for nonlinear systems represented by input-output models," *IEEE Transactions on Industrial Electronics*, vol. 67, no. 2, pp. 1222-1232, 2019.

[19] J. Huang, M. Zhang, S. Ri, C. Xiong, Z. Li, and Y. Kang, "High-order disturbance-observer-based sliding mode control for mobile wheeled inverted pendulum systems," *IEEE Transactions on Industrial Electronics*, vol. 67, no. 3, pp. 2030-2041, 2019.

[20] H. Rabiee, M. Ataei, and M. Ekramian, "Continuous nonsingular terminal sliding mode control based on adaptive sliding mode disturbance observer for uncertain nonlinear systems," *Automatica*, vol. 109, 108515, 2019.

[21] B. Xu, "Composite learning finite-time control with application to quadrotors," *IEEE Transactions on Systems, Man, and Cybernetics: Systems*, vol. 48, no. 10, pp. 1806-1815, 2017.

[22] Y. Yang, T. Dai, C. Hua, and J. Li, "Composite nns learning full-state tracking control for robotic manipulator with joints flexibility," *Neurocomputing*, vol. 409, pp. 296-305, 2020.

[23] M. Li, Y. Chen, and Y. Liu, "Adaptive disturbance observer-based event-triggered fuzzy control for nonlinear system," *Information Sciences*, vol. 575, pp. 485-498, 2021.

[24] M. Van and S. S. Ge, "Adaptive fuzzy integral sliding-mode control for robust fault-tolerant control of robot manipulators with disturbance observer," *IEEE Transactions on Fuzzy Systems*, vol. 29, no. 5, pp. 1284-1296, 2020.

[25] S. Ding, J. Peng, H. Zhang, and Y. Wang, "Neural network-based adaptive hybrid impedance control for electrically driven flexible-joint robotic manipulators with input saturation," *Neurocomputing*, vol. 458, pp. 99-111, 2021.

[26] S. Ling, H. Wang, and P. X. Liu, "Adaptive fuzzy tracking control of flexible-joint robots based on command filtering," *IEEE Transactions on Industrial Electronics*, vol. 67, no. 5, pp. 4046-4055, 2019.

[27] W. Chang, Y. Li, and S. Tong, "Adaptive fuzzy backstepping tracking control for flexible robotic manipulator," *IEEE/CAA Journal of Automatica Sinica*, vol. 8, no. 12, pp. 1923-1930, 2021.

[28] C. Liu, X. Xiang, and P. Poignet, "Adaptive tracking control of rigid-link flexible-joint robot manipulator with uncertainties," *IFAC Proceedings Volumes*, vol. 44, no. 1, pp. 10300-10306, 2011.

[29] X. Chen, T. Huang, J. Cao, J. H. Park, and J. Qiu, "Finite-time multi-switching sliding mode synchronisation for multiple uncertain complex chaotic systems with network transmission mode," *IET Control Theory & Applications*, vol. 13, no. 9, pp. 1246-1257, 2019.

[30] C. Ren and S. He, "Sliding mode control for a class of nonlinear positive markov jumping systems with uncertainties in a finite-time interval," *International Journal of Control, Automation, and Systems*, vol. 17, no. 7, pp. 1634-1641, 2019.

[31] A. K. Junejo, W. Xu, C. Mu, M. M. Ismail, and Y. Liu, "Adaptive speed control of pmsm drive system based a new sliding-mode reaching law," *IEEE Transactions on Power Electronics*, vol. 35, no. 11, pp. 12110-12121, 2020.

[32] A. K. Junejo, W. Xu, C. Mu, and Y. Liu, "Improved continuous fast terminal sliding mode control for speed regulation of surface-mounted permanent magnet synchronous motor," *Proc. of 21st International Conference on Electrical Machines and Systems (ICEMS)*, IEEE, pp. 93-98, 2018.

[33] S. Shi, J. Gu, S. Xu, and H. Min, "Globally fixed-time high-order sliding mode control for new sliding mode systems subject to mismatched terms and its application," *IEEE Transactions on Industrial Electronics*, vol. 67, no. 12, pp. 10776-10786, 2019.

[34] S. Ullah, A. Mehmood, Q. Khan, S. Rehman, and J. Iqbal, "Robust integral sliding mode control design for stability enhancement of under-actuated quadcopter," *International Journal of Control, Automation, and Systems*, vol. 18, no. 7, pp. 1671-1678, 2020.

[35] J. Lu, S. Yu, G. Zhu, Q. Zhang, C. Chen, and J. Zhang, "Robust adaptive tracking control of umsvs under input saturation: A single-parameter learning approach," *Ocean Engineering*, vol. 234, 108791, 2021.

[36] B. Huang, S. Song, C. Zhu, J. Li, and B. Zhou, "Finite-time distributed formation control for multiple unmanned surface vehicles with input saturation," *Ocean Engineering*, vol. 233, 109158, 2021.

[37] Z. Li, C.-Y. Su, L. Wang, Z. Chen, and T. Chai, "Nonlinear disturbance observer-based control design for a robotic exoskeleton incorporating fuzzy approximation," *IEEE Transactions on Industrial Electronics*, vol. 62, no. 9, pp. 5763-5775, 2015.

[38] L. Tang and D. Li, "Time-varying barrier lyapunov function based adaptive neural controller design for nonlinear pure-feedback systems with unknown hysteresis," *International Journal of Control, Automation, and Systems*, vol. 17, no. 7, pp. 1642-1654, 2019.

[39] C. Li, W. Cui, D. Yan, Y. Wang, and C. Wang, "Adaptive dynamic surface control of a flexible-joint robot with parametric uncertainties," *Scientia Iranica*, vol. 26, no. 5, pp. 2749-2759, 2019.

[40] K. P. Tee, S. S. Ge, and E. H. Tay, "Barrier lyapunov functions for the control of output-constrained nonlinear systems," *Automatica*, vol. 45, no. 4, pp. 918-927, 2009.

Quanwei Wen received his B.E. degree in electrical engineering and its automation from Dalian Jiaotong University, Dalian, China, in 2015. Now, he is pursuing an M.E. degree in electric engineering in Nanchang University. His current research interests include sliding mode control, neural network control, and backstepping control of robotic manipulator with flexible joint.

Xiaohui Yang received his B.Sc., M.Sc., and Ph.D. degrees from Nanchang University, Nanchang, China, in 2003, 2006, and 2015, respectively. He has been with the Department of Electronic Information Engineering, School of Information Engineering, Nanchang University, since 2006, where he is currently an Associate Professor. His current research interests include intelligent control and stochastic non-linear systems.

Chao Huang received her B.E. degree in electrical engineering and its automation from Nanchang Institute of Technology, Nanchang, China, in 2020. Now, she is pursuing an M.E. degree in electric engineering in Nanchang University. Her current research interests include sliding mode control, neural network control, adaptive non-linear control of robotic manipulator, and control of circuit-breaker phase selection closing.

Junping Zeng received her B.E. degree in electrical engineering and its automation from Minnan Normal University, China, in 2020. Now, she is pursuing an M.E. degree in electric engineering in Nanchang University. Her current research interests include sliding mode control and combined CCHP microgrids with integrated demand response.

Zhixin Yuan received his B.E. degree in electrical engineering and its automation from East China Jiaotong University, Nanchang, China, in 2020. Now, he is pursuing an M.E. degree in electric engineering in Nanchang University. He current research interests include optimal configuration of microgrid and grid-connected technology of microgrid.

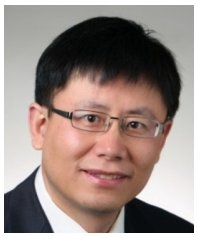

Peter Xiaoping Liu received his B.Sc. and M.Sc. degrees from Northern Jiaotong University, China in 1992 and 1995, respectively, and a Ph.D. degree from the University of Alberta, Canada in 2002. He has been with the Department of Systems and Computer Engineering, Carleton University, Canada since July 2002, and he is currently a Professor and Canada Research Chair. His research interests include interactive networked systems and teleoperation, haptics, micro-manipulation, robotics, and intelligent systems. Dr. Liu is a licensed member of the Professional Engineers of Ontario (P.Eng), a senior member of IEEE and Fellow of Engineering Institute of Canada (FEIC).